Measurement 121 (2018) 1–5

Contents lists available at ScienceDirect

Measurement

journal homepage: www.elsevier.com/locate/measurement

Measurements of photorefractive birefringence on the different propagation directions in electro-optic crystals

Ruey-Ching Twu*, Yi-Fan Chu

Department of Electro-Optical Engineering, Southern Taiwan University of Science and Technology, No. 1 Nan-Tai Street, Yungkang, Tainan 71005, Taiwan

ARTICLE INFO

Keywords:
Photorefractive effect
Birefringence
Electro-optic crystals

ABSTRACT

A single-beam pump-probe method based on a dual-channel phase measurement system was adopted to measure photo-induced phase variations caused by the photorefractive effect. This study systematically studied the dependence of photorefractive birefringence on the propagation directions of probing lights in various electro-optic crystals at visible wavelengths.

1. Introduction

Optical materials with a photorefractive effect have been studied in various photonic applications [1–4]. For example, an optical hologram storage system needs highly photo-sensitive materials to recode the information grating induced by the photo-induced spatial phase grating; however, nonlinear optic and electro-optic (EO) devices prefer low photo-sensitivity for stable operations [5,6]. Therein, the photorefractive effect causes a phase mismatch between the pump and the converted wavelengths, and the conversion efficiency is reduced in nonlinear optic devices. The refractive index change also creates unstable phase modulations in the intensity of electro-optic modulators [6]. It is well known that all electro-optic modulators generate some unwanted residual amplitude modulation that degrades the performance of the system and ultimately limits its usefulness. Moreover, the phase drifted by the photorefractive effect will cause the bias voltage to be changed in an integrated lithium niobate (LN) gyro chip [7]. In the past decades, different analyzing methods have been used to explore the photorefractive effect in bulk crystals, planar waveguides, and channel waveguides [8–14]. The two-beam coupling method used to form a periodical refractive index grating has been widely used to evaluate photorefractive properties in photo-sensitive crystals [8,9]. Spatial refractive index grating can deflect an oblique incident light beam into multiple exiting beams due to the diffraction phenomenon. The diffraction efficiency of the first order light is dependent on the refractive index change caused by the photorefractive effect. The recoding and erasing periods can be easily monitored using this method; however, it has a limited effect on crystal directions. To form the spatial refractive index grating, a single-beam technique based on Ronchi-grating-based measurement used to monitor diffraction efficiency in photo-sensitive crystals under different input powers was successfully demonstrated [10]. Since serious photo-induced refractive index variations will change the propagation properties of the probing beam, a single-beam pump-probe method was used. This measures distortions of the beam profile in doped lithium tantalate (LT) crystals containing different impurities at a highly irradiated intensity [11]. Moreover, this method has been implemented to determine damage thresholds in annealed proton exchanged LN planar waveguides [12]. The intensity threshold was defined by the incoupled intensity Iin, at which the outcoupled intensity Iout is no longer proportional to Iin. A Mach-Zehnder interferometer was adopted to study the photorefractive behavior in different orientations of LN crystals [13]. The dynamic refractive index changes could be observed according to the time-varied interferometric patterns. The Mach-Zehnder interferometric technique has also proved to be a useful complementary tool for characterizing optical damage in the planar waveguide [12]. However, fine optical alignments are needed in the splitting-path interferometer for such bulk and planar waveguide devices [12,13]. Since the phase difference in the interferometer is dependent on an optical path difference, an integrated asymmetrical Mach-Zehnder waveguide interferometer was used to measure photorefractive phenomenon utilizing a short-wavelength pump and long-wavelength probe method [14]. In a simple common-path interferometer, measurement of the photorefractive phase shift is evaluated by polarization interferometry [15]. According to relationships between the measured phase variations and the photorefractive birefringence, the photorefractive effect can be further analyzed. In addition, LN substrates can produce different kinds of integrated EO devices depending on crystal direction. For example, the propagation direction along an extraordinary refractive index axis (ne-axis) can be used for a polarization converter [16], and the phase matching

* Corresponding author.
E-mail address: rctwu@stust.edu.tw (R.-C. Twu).

https://doi.org/10.1016/j.measurement.2018.02.042
Received 17 April 2017; Received in revised form 6 February 2018; Accepted 21 February 2018
Available online 22 February 2018
0263-2241/

conditions are important for obtaining stable conversion efficiency. The propagation direction perpendicular to the ne-axis was used for high-speed phase and intensity modulators [7].

Recently, a homemade lithium niobate Zn-indiffused phase modulator (ZIPM) with a stable phase operation was successfully demonstrated in measuring common-path phase retardations based on the homodyne and heterodyne metrologies at wavelengths of 532 nm and 632.8 nm [17,18]. The dual-channel arrangements were adopted to suppress the common phase noise from the residual photorefractive impacts [19]. Therefore, the creation of a photosensitive measurement instrument has been proposed to evaluate the power dependent characteristics at a wavelength of 532 nm [20].

In this paper, a probing beam with focus and phase modulated from the ZIPM was successfully applied to the photorefractive birefringence measurements of various EO materials. The simple common path arrangement and LabVIEW-based phase-interrogation scheme provided flexible measurements. The probing beam with low divergence was easily transmitted through the thin planar substrate with a long distance of over 18 mm. Thick crystal and thin wafer EO materials were used to study the photorefractive effect depending on the propagation directions. Photorefractive effects are deeply related to the doped impurity as well as to the wavelengths of irradiated light. Usually, shorter wavelengths can more easily make the essential photorefractive. Therefore, the proposed simple and flexible instrument is important for analyzing the photorefractive effect through measurements of photorefractive birefringence for such photo-sensitive materials.

2. Measurement setup and principle

The schematic diagram of the dual-channel phase measurement setup for photorefractive birefringence analysis in homodyne metrology is shown in Fig. 1 [19]. The ZIPM was fabricated in the x-cut/z-propagating LN substrate as reported in [17]. The width and length of the fabricated channel waveguide were 4 μm and 22 mm, respectively. The length and gap of the parallel electrodes were 12 mm and 14 μm, respectively. A diode pumped solid state (DPSS) laser (532 nm) and a helium–neon laser (632.8 nm) were used for the measurements. The optimum waveguide fabrications were able to obtain a singly guided mode for both orthogonal polarizations with wavelengths of 532 nm and 632.8 nm. The input power was controlled using an attenuator (AT). A polarizer (PL) was used to obtain a probe light with equal intensities in both orthogonal polarizations. The input power was coupled into the ZIPM through object lens L1 because the power intensities applied to the test crystals were dependent on the beam sizes, which could be adjusted after passing through another object, lens L2. After undergoing a beam splitter (BS), the transmitted sensing light was used as a probing light to measure the phase variations through the test EO crystals (EO). The inset shows the different propagation directions for the probing lights in the EO crystals, in which kne and kno represent the propagation directions that are parallel and perpendicular to the ne-axis of the EO crystals, respectively. At the same time, the reflected light was adopted as a reference light for monitoring the phase variation from the ZIPM due to slight photorefractive birefringence impacts. After

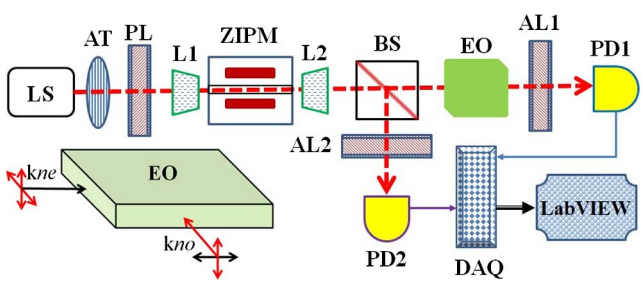

Fig. 1. Schematic diagram of the Photorefractive birefringence measurement setup.

analyzers AL1 and AL2, the corresponding sensing and reference interferometric signals were detected by photodetectors PD1 and PD2. The dual channel voltages were connected to a data acquisition device (DAQ), and were analyzed on a LabVIEW platform.

The LN and LT had the same crystal symmetry (trigonal, 3m) and belonged to a uniaxial birefringence crystal. The photo-excited charges were generated, and rearrangements of the free charges were deeply dependent on two driving forces, including the drift and diffusion effects. In case of the kno probing light, the inherent dipole force caused the freely negative charges to drift in a parallel fashion along the ne-axis. The non-uniform distributions of the negative charges easily formed a net spatial charge field. In case of the kne probing light, the diffusion ability of the freely negative charge was proportional to a gradient of the carrier concentration. It is difficult to form a net spatial charge field without the dipole force. Both of the spatial fields were able to induce the refractive index change through EO effects. The photorefractive birefringence (PB) from the kno probing light is represented by:

$$\Delta n_{PB}^{o} = \frac{1}{2}\cdot(n_e^3\cdot r_{33} - n_o^3\cdot r_{13})\cdot E_{SC}^{o}, \tag{1}$$

where ne and no are the extraordinary refractive index and ordinary refractive index, respectively; r_{33} and r_{13} are the EO coefficients; and E_{SC}^{o} is a spatial charge field parallel to the ne-axis. The PB from the kne probing light is represented by:

$$\Delta n_{PB}^{e} = (n_o^3\cdot r_{22})\cdot E_{SC}^{e}, \tag{2}$$

where r_{22} is the EO coefficient; and E_{SC}^{e} is a spatial charge field perpendicular to the ne-axis. The measured phase variation is given by:

$$\Delta\phi = \frac{2\pi}{\lambda}\cdot L\cdot\Delta n_{PB}, \tag{3}$$

where λ is the probe wavelength, and L is the probing crystal length. According to the measured Δϕ, PB is defined as:

$$\Delta n_{PB} = \frac{\lambda}{2\pi\cdot L}\cdot\Delta\phi. \tag{4}$$

3. Results and discussions

Fig. 2 shows the TE guided mode profiles for wavelengths of 532 nm and 632.8 nm. The TM modal profiles were similar to the TE modes. The beam diameter R was simply defined as a half width of the maximum intensity of the modal profile. The measured values of the beam diameter were approximately 190 μm and 240 μm for the wavelengths of 532 nm and 632.8 nm, respectively. Moreover, the beam area (A) was roughly defined as $A = \pi \times (R/2)^2$. The intensity was defined as power per unit area. At the same input power of 25 μW, the irradiated intensities were about 88 and 55 mW/cm^2 for the probing wavelengths of 532 nm and 632.8 nm, respectively. In this study, three different kinds of LN crystals were used for measurements. These bulk-type crystals included congruently melting undoped material (CLN), 1.5% mol Fe-doped material (Fe:CLN), and 5.0% mol MgO-doped material (MgO:CLN). Fig. 3 shows the phase variations on the dual channels and the net phase variations after subtractions between them under a probe light with a 532 nm wavelength. Fig. 3(a) gives the similar phase trends for both channels over a measurement period of 10 min. The bulk-type CLN with a length of 5 mm was placed on the sensing path. Under a probing light that was parallel to the ne-axis, the maximum phase variations after subtractions were 0.5 deg at an irradiated power of 40 μW, as shown in Fig. 3(b). According to Eq. (4), the corresponding photorefractive birefringence was 2.03×10^{-6} refractive index units (RIU). Therefore, measurements and calculations of photorefractive birefringence variations were used to further study the dependence on the propagation directions and doped impurities in the LNs.

Fig. 4 gives the measured photorefractive birefringence variations

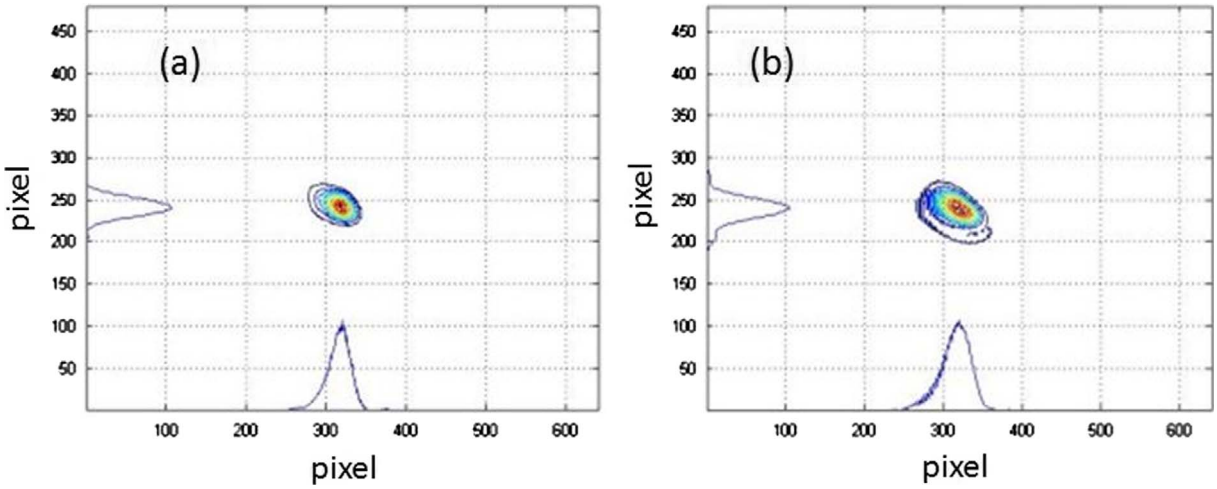

Fig. 2. TE beam profiles for different wavelengths: (a) 532 nm; and (b) 632.8 nm.

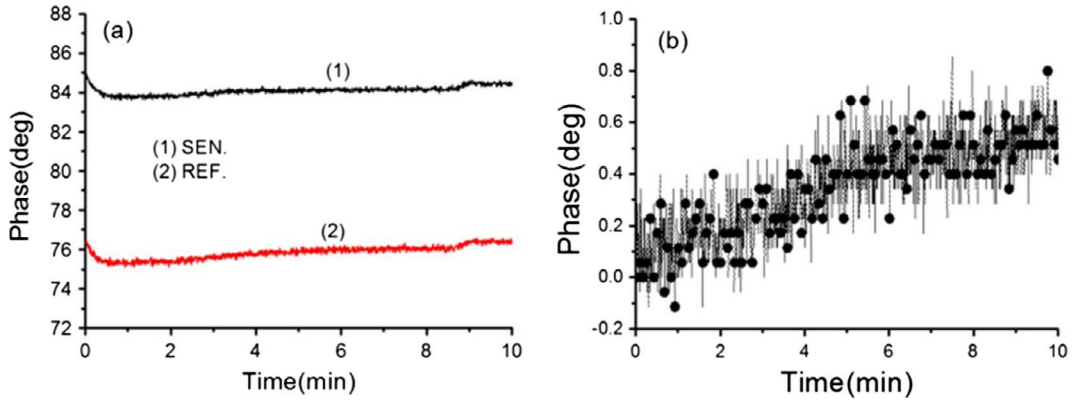

Fig. 3. Phase measurements in a measurement period of 10 min for (a) dual channels; and (b) subtracted results between two channels for the 532 nm wavelength.

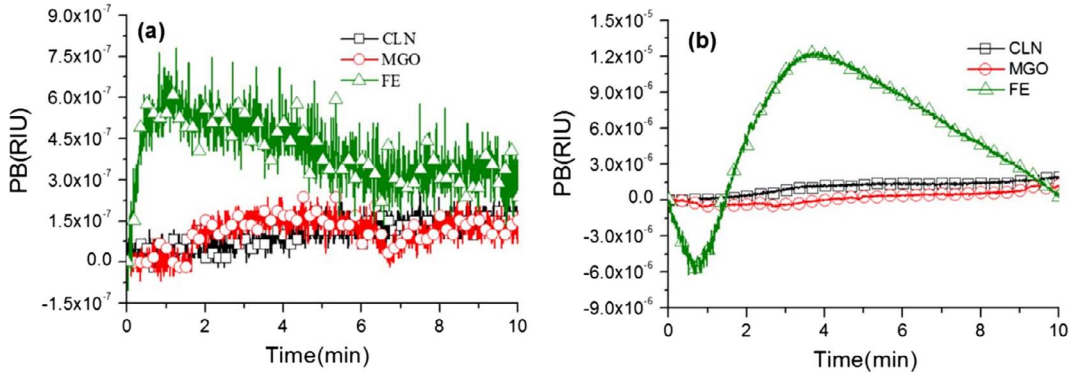

Fig. 4. Photorefractive birefringence variations for the three LNs measured at a wavelength of 532 nm on different propagation directions: (a) kne probing light; and (b) kno probing light.

over a period of 10 min for different propagating directions in three different bulk-type LN crystals under a probing light with a 532 nm wavelength. Fig. 4(a) shows the results for the kne probing light, in which the maximum birefringence changes were 6.81×10^{-7}, 1.94×10^{-7}, and 1.92×10^{-7} RIU for the Fe:CLN, CLN, and MgO:CLN, respectively. In case of the kno probing lights, as shown in Fig. 4(b), the maximum birefringence changes were 1.81×10^{-5}, 2.03×10^{-6}, and 1.27×10^{-6} RIU for the Fe:CLN, CLN, and MgO:CLN, respectively. According to the measurement results, the birefringence change of Fe:CLN on the kno probing light was 26 times larger than that of the kne probing light under the same measurement periods and input powers. As shown in Fig. 4(b), the photorefractive birefringence minimum occurred at about one minute, which was probably caused by the residual charges in the Fe-doped LN after the experiments had been performed numerous times. Once the input light erased the exited charge distributions in the initial stage, the photo-excited carriers accumulated continually on the edge of the propagation beam to form the spatial electric field again.

In comparison with the probing light with a 532 nm wavelength, the probing light with a 632.8 nm wavelength and a higher input power of 60 μW was used to study the photorefractive birefringence changes, as shown in Fig. 5. Fig. 5(a) shows the results for the kne probing lights, in which the maximum birefringence changes were 7.92×10^{-7}, 3.13×10^{-7}, and 3.83×10^{-7} RIU for the Fe:CLN, CLN, and MgO:CLN, respectively. The photorefractive birefringence difference was slight between the CLN and MgO:CLN. In the case of the kno

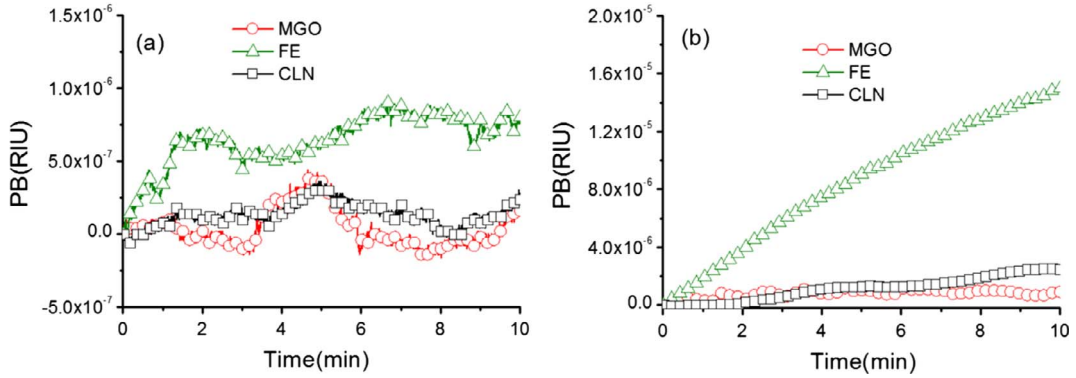

Fig. 5. Photorefractive birefringence variations for the three LNs measured at a wavelength of 632.8 nm on different propagation directions: (a) kne probing light; and (b) kno probing light.

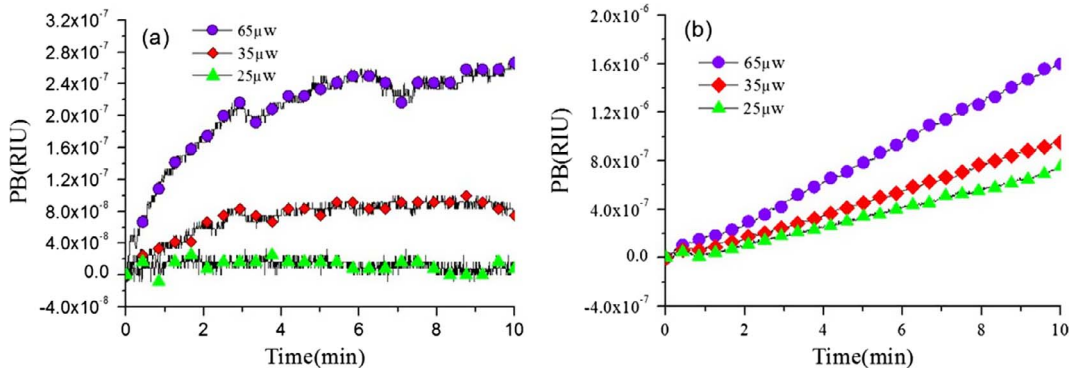

Fig. 6. Photorefractive birefringence variations for different input powers in the x-cut CLN planar sample: (a) kne probing light; and (b) kno probing light.

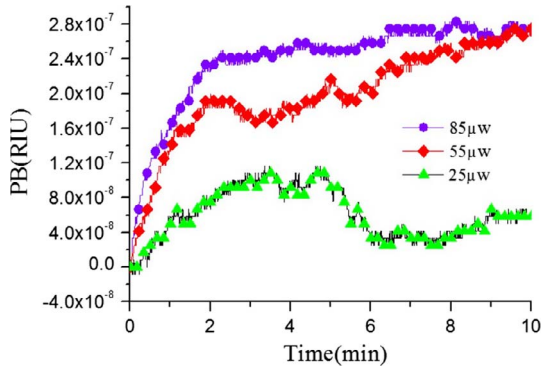

Fig. 7. Photorefractive birefringence variations measured by the kno probing light for different input powers in the z-cut wafer-type LT sample.

probing lights, as shown in Fig. 5(b), the maximum birefringence changes were 1.52×10^{-5}, 2.54×10^{-6}, and 1.83×10^{-6} RIU for the Fe:CLN, CLN, and MgO:CLN, respectively. The birefringence change of Fe:LN on the kno probing light was 19 times larger than that of the kne probing light used with the same measurement times and input powers. According to the measurement results of Figs. 4 and 5, essential photorefractive birefringence differences were observed that were deeply dependent on the doped impurities, the propagation directions, and the probing wavelengths. Moreover, the magnitude of the spatial electric field causing photorefractive birefringence was mainly decided by the number of photo-excited carriers. The photo-excited carriers decreased in the MgO-doped LN crystal, in comparison with the non-doped LN crystal at the same wavelength and probing light power; however the photo-excited carriers dramatically increased in the Fe-doped LN crystal. Therefore, the Fe-doped LN crystal easily achieved high photorefractive birefringence in both the kno and kne probing directions.

To further evaluate the capability of the focused and low divergence probing beam for photorefractive birefringence measurements, bulk samples were replaced with wafer-type EO plates. In the planar-type CLN and LT samples, both with a thickness of 1 mm, the end faces of the samples were polished to reduce surface scattering of the probing light. The test samples were placed on a precision stage for fine alignment. In the planar LN samples, the propagation lengths were 12 mm and 18 mm for the kne and kno probing lights, respectively. Fig. 6 shows the measurement results for two orthogonal probing directions in the x-cut CLN substrate. Fig. 6(a) shows the results obtained using the kne probing light, in which the maximum birefringence changes were 2.52×10^{-7} and 8.54×10^{-8} RIU for the input powers 65 μW and 35 μW, respectively. In the initial period, the birefringence values showed exponential growth for the sufficient input powers. The birefringence variations were smaller than 2.04×10^{-8} RIU with an input power of 25 μW. The detection limitation of the photorefractive birefringence was around 2×10^{-8} RIU and represented the measurement accuracy in the proposed measurement system. The same input powers yielded measurement results for the kno probing lights, as shown in Fig. 6(b). In comparison with the results shown in Fig. 6(a), the birefringence values rapidly increased for the three powers. During the measurement period of 10 min, the birefringence values did not become fully saturated, and the maximum values were 1.72×10^{-6}, 9.43×10^{-7}, and 7.27×10^{-7} RIU for the input powers 65 μW, 35 μW and 25 μW, respectively. The higher input power resulted in a larger rate of increase, and the values of the photorefractive birefringence change were at least 10 times larger than the results shown in Fig. 6(a). The birefringence change rate, as well as the saturation value, are dependent on the input wavelength and power of the probing light. Typically, the maximum birefringence change at the saturation period is used to characterize the photorefractive effect. In addition, the photorefractive sensitivity can be calculated by considering the birefringence change rates in the initial stage, as described in the researchers'

previous study [20], and this is the basis for using 10 min for each experiment.

Fig. 7 shows the photorefractive birefringence measurement results for the kno probing light in a z-cut wafer-type LT sample under different input powers. At the propagation length of 12 mm, the maximum values of birefringence were 2.85×10^{-7}, 2.73×10^{-7} and 1.18×10^{-7} RIU for the input powers 85, 55 and 25 μW, respectively. The photorefractive birefringence levels were the same as those attained using the kne probing light in the CLN substrate under similar input powers.

4. Conclusions

This paper presented a simple and flexible phase interrogation instrument for measuring photorefractive birefringence using a single-beam pump-probe method. The low divergence and focused beam with low applied voltages for phase modulations could pass easily through the thin wafer sample in the homodyne interferometer. According to the measured phase variations, the photorefractive birefringence obtained was able to reflect dynamic space charge formations due to the photorefractive effect in different EO crystals. The values of the photorefractive birefringence according to the different propagation directions and input powers were measured using 532 nm and 632.8 nm wavelengths.

Acknowledgements

This study was supported in part by the Ministry of Science and Technology in Taiwan under grant number MOST 104-2221-E-218-027.

References

[1] P. Gunter, J.-P. Huignard, Photorefractive Materials and Their Applications 2, Springer, Berlin, 2006.
[2] M. Imlau, S. Haussühl, T. Woike, R. Schieder, V. Angelov, R.A. Rupp, K. Schwarz, Holographic recording by excitation of metastable electronic states in Na2[Fe(CN) 5NO]·2H2O: a new photorefractive effect, Appl. Phys. B 68 (1999) 877–885.
[3] E. Hata, K. Mitsube, K. Momose, Y. Tomita, Holographic nanoparticle-polymer composites based on step-growth thiol-ene photopolymerization, Opt. Mater. Express 1 (2011) 207–222.
[4] J. Marion, Strengthened solid-state laser materials, Appl. Phys. Lett. 47 (1985) 694–696.
[5] M. Asobe, O. Tadanaga, T. Yanagawa, H. Ito, H. Suzuki, Reducing photorefractive effect in periodically poled ZnO- and MgO-doped $LiNbO_3$ wavelength converters, Appl. Phys. Lett. 78 (2001) 3163–3165.
[6] J. Sathian, E. Jaatinen, Intensity dependent residual amplitude modulation in electro-optic phase modulators, Appl. Opt. 51 (2012) 3684–3691.
[7] E.L. Wooten, K.M. Kissa, A. Yi-Yan, E.J. Murphy, D.A. Lafaw, P.F. Hallemeier, D. Maack, D.V. Attanasio, D.J. Fritz, G.J. McBrien, D.E. Bossi, A review of lithium niobate modulators for fiber-optic communications systems, IEEE J. Select. Top. Quant. Electron. 6 (2000) 69–82.
[8] E.J. Kim, H.R. Yang, S.J. Lee, G.Y. Kim, C.H. Kwak, Orientational photorefractive holograms in porphyrin: Zn-doped nematic liquid crystals, Opt. Express 16 (2008) 17329–17341.
[9] Y. Liu, L. Liu, D. Liu, L. Xu, C. Zhou, Intensity dependence of two-center nonvolatile holographic recording in $LiNbO_3$: Cu: Ce crystals, Opt. Commun. 190 (2001) 339–343.
[10] I. de Oliveira, J. Frejlich, Ronchi-grating-based measurement of photorefractive recording response time, Opt. Lett. 37 (2012) 277–279.
[11] Peixiong Zhang, Jigang Yin, Shuaiyi Zhang, Rui Zhang, Lianhan Zhang, Youchen Liu, Xu. Jianqiu, Yin Hang, Crystal growth, spectroscopic characterization, and laser operation of Tm/Mg: $LiTaO_3$ crystal, Opt. Mater. Express 4 (2014) 255–265.
[12] F. Luedtke, J. Villarroel, A. García-Cabañes, K. Buse, M. Carrascosa, Correlation between photorefractive index changes and optical damage thresholds in z-cut proton-exchanged-$LiNbO_3$ waveguides, Opt. Express 17 (2009) 658–665.
[13] I. Turek, N. Tarjányi, Investigation of symmetry of photorefractive effect in $LiNbO_3$, Opt. Express 15 (2007) 10782–10788.
[14] T. Fujiwara, R. Srivastava, X. Cao, R.V. Ramaswamy, Comparison of photorefractive index change in proton-exchanged and Ti-diffused $LiNbO_3$ waveguides, Opt. Lett. 18 (5) (1993) 346–348.
[15] R.K. Ing, J.-P. Monchalin, Measurement of the photorefractive phase shift by polarization interferometry, Opt. Lett. 18 (1993) 852–854.
[16] Suwat Thaniyavarn, Wavelength-independent, optical-damage-immune $LiNbO_3$ TE–TM mode converter, Opt. Lett. 11 (1986) 39–41.
[17] R.C. Twu, H.Y. Hong, H.H. Lee, An optical homodyne technique to measure photorefractive-induced phase drifts in lithium niobate phase modulators, Opt. Express 16 (2008) 4366–4374.
[18] R.C. Twu, Y.H. Lee, H.Y. Hou, A comparison between two heterodyne light sources using different electro-optic modulators for optical temperature measurements at visible wavelengths, Sensors 10 (2010) 9609–9619.
[19] R.C. Twu, H.Y. Hong, H.H. Lee, Dual-channel optical phase measurement system for improved precision, Opt. Lett. 33 (2008) 2530–2532.
[20] R.C. Twu, Y.F. Chu, M.T. Hsu, A simple instrument for measuring the light-induced birefringence in a photorefractive crystal, Microwave Opt. Tech. Lett. 53 (2011) 367–369.